Stereo Vision Combined with Laser Profiling for Mapping of Pipeline Internal Defects

Amal Gunatilake, *Member, IEEE*, Lasitha Piyathilaka, *Member, IEEE*, Antony Tran, Vinoth Kumar Viswanathan, *Member, IEEE*, Karthick Thiyagarajan, *Member, IEEE*, Sarath Kodagoda, *Member, IEEE*

***Abstract*— Underground potable water pipes are essential infrastructure assets for any country. A significant proportion of those assets are deteriorating due to pipe corrosion which results in premature failure of pipes causing enormous disruptions to the public and loss to the economy. To address such adverse effects, the water utilities in Australia exploit advanced pipelining technologies with a motive of extending the service life of their pipe assets. However, the linings are prone to defects due to improper liner application and unfavorable environmental conditions during the liner curing phase. To monitor the imperfections of the pipe linings, in this article, we propose a mobile robotic sensing system that can scan, detect, locate and measure pipeline internal defects by generating three-dimensional RGB-Depth maps using stereo camera vision combined with infrared laser profiling unit. The system does not require complex calibration procedures and it utilizes orientation correction to provide accurate real-time RGB-D maps. The defects are identified and color mapped for easier visualization. The robotic sensing system was extensively tested in laboratory conditions followed by field deployments in buried water pipes in Sydney, Australia. The experimental results show that the RGB-D maps were generated with millimeter (mm) level accuracy with demonstrated liner defect quantification.**

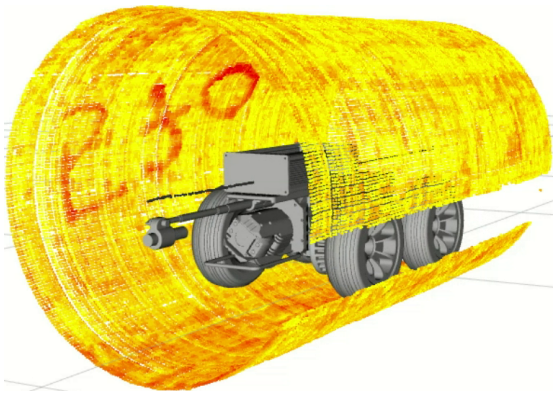

***Index Terms*— 3D laser profiling, Defects detection, Mobile robot, Pipeline inspection, RGB depth mapping, Robotic sensing, Robotic vision, Stereo camera vision, Water pipes**

I. Introduction

Underground infrastructures such as water and waste water pipes undergo severe metallic [1] and concrete [2], [3] corrosion with age. The metallic pipes show both external and internal corrosion either as patches or pits. This results in reduction of their service life, which can lead to disastrous water pipe bursts and sewer collapses [4]. Replacements of corroded pipes are generally expensive and hence water utilities adopt different lining technologies such as spray liners and cured-in-place pipe (CIPP) liner that can add a protective semi-structural layer to mitigate the effects of corrosion. However, those lining technologies can fail over time due to poor application and environmental conditions. A survey conducted as a part of our collaborative project among line manufacturers, applicators, researchers, and water utilities identified the liner imperfections to be the most crucial liner defects to be concerned. The liner imperfections include folds, wrinkles, dimples, and bulges in pipelines. The pipes being mostly underground, timely monitoring and fit for purpose renewals to avoid failures are significant challenges for water utilities around the world. Solutions such as embedded sensors in pipes to monitor their condition are still futuristic [5]. Human entries to such tiny confined spaces for visual and physical inspections are mostly impossible and associated with high health and safety risks. Traditional methods such as robots with CCTV (closed circuit television) inspection cameras fail to provide critical structural information to make accurate decisions to maintain the underground infrastructure.

There has been few attempts in the past to explore the use of various sensing technologies for 3D reconstruction of the internal surface of underground infrastructure such as using LiDAR (light detection and ranging) technology used in large diameter pipes and tunnels [6]. They require centimeter level accuracy [7] which limits the applicability for small diameter pipes requiring sub-centimeter accuracy. Further the LiDAR sensors do not provide color information and therefore, external cameras with proper calibrations

Manuscript received XXXXXXX XX, 2020; revised XXXXXX XX, 2020; accepted XXXXXXX XX, 2020. This work was supported by the Smart Linings for Pipes and Infrastructure project funded by the Australian Federal Government through the Cooperative Research Centres Projects (CRC-P) grant. The associate editor coordinating the review of this article and XXXXXXXXX it for publication was XXXXXXXXXXXXXXX. (*Corresponding author: Amal Gunatilake.*)

All the authors are with the iPipes Lab, UTS Robotics Institute, Faculty of Engineering and Information Technology, University of Technology Sydney, Sydney, NSW 2007, Australia (e-mail: amal.d.gunatilake@student.uts.edu.au; Lasitha.Piyathilaka@uts.edu.au; Antony.Tran@uts.edu.au; Vinothkumar.Viswanathan@uts.edu.au; Karthick.Thiyagarajan@uts.edu.au; Sarath.Kodagoda@uts.edu.au).

are required for overlaying color information on 3D point clouds. Structured 3D cameras like Intel Real-sense [8] are heavily used in robotics to generate 3D point cloud maps in indoor environments. However, they can't achieve millimeter level accuracy which is required for detecting small defects in small diameter pipes [9]–[11].

In recent years, laser profiling with monocular vision has been exploited to generate three-dimensional (3D) maps of internal surfaces of pipelines providing informative structural information of the pipes [12]–[15]. Compared to CCTV, this emerging technology is capable of quantifying structural defects or ovality changes in pipes. However, laser profiling with a monocular camera needs extensive field calibration and hey suffere from lateral movements which cause errors in 3D reconstruction. Most of these technologies process data offline limiting real time opportunistic decision making ability such as targeting suspicious areas and re-scanning areas of missing data.

3D laser profiling with a laser ring projector and a single camera is the preferred method of use by many water utilities to generate 3D profiles of pipes [14], [16], [17]. In this method, a laser ring projector is mounted in front of a camera that projects a continuous red laser ring on to the pipe surface [17]–[19]. This system is mounted on a robotic platform and moved inside the pipe. The small deviations of the laser ring caused by defects of the pipe surface are detected by the camera and simple trigonometry is used to generate the 3D point cloud. However, with unavoidable movement disturbances, these systems tend to introduce large errors in 3D reconstruction. They generally need onsite calibration and do not provide color information [20].

In this paper, we propose an improved laser profiling system that uses stereo camera vision with IR (infrared) laser-pattern projection to overcome the limitations discussed above. The proposed stereo camera vision technique enables to modify the depth measurements of the laser projection to compensate for lateral movements of the robot leading to increased accuracy of the 3D reconstruction. Unlike conventional mono camera vision-based laser profiling, stereo camera vision system does not need field calibration at each deployment. Therefore, it can be used efficiently in wide range of pipe diameters with multiple deployments. The proposed system is capable of generating 3D point clouds of pipes in real-time while traversing through the pipelines. We use an IR laser beam instead of the traditional red color laser beam so as to extract real colors of the pipe surface. Two IR cameras are used for stereo vision processing and 3D reconstruction. The calibrated RGB (red green blue) camera provides the true color for the 3D reconstruction. The data is further processed to generate a color heat map for defects and ovality variations of the pipe surfaces. This allows visualization of the internal pipe defects in real-time.

The key contributions of the paper are:

- Firstly, we propose a stereo vision-based laser profiling system integrated with the mobile robotic platform for real-time RGB-Depth mapping with true color information extracted from the pipelines using color and IR cameras. The proposed approach requires only one-time calibration and generates RGB-D maps with 1mm accuracy for pipe diameters ranging from 400mm to 700mm.
- Secondly, our system generates heat-maps that highlight and measure defected areas in scanned pipelines which enables easy monitoring of damaged areas and the evolution of them in the long term.
- Thirdly, the stereo vision is utilized for detecting the orientation of the robot by determining yaw and pitch parameters, which assists in accurate RGB-D map building.

The rest of this article is structured as follows: Section II and III describe various algorithms, hardware and software architectures. The experimental results are presented in Section IV with discussions and finally, Section V concludes the article by summarizing the key outcomes and briefs the intended future work.

II. 3D Data Generation And Processing

This section describes various algorithms used in the 3D data generation and processing execution pipeline as is shown in Appendix Fig. 1. The camera images with calibration parameters are fed into the image processing algorithms to filter laser projection for 3D point cloud generation. The odometry errors are corrected using orientation detection algorithms. Using the circle detection and ray casting algorithms, a heat map is generated by detecting the ovality changes to highlight the defects.The 3D point cloud receives the colors extracted from the RGB image.

1) Camera calibration: Camera calibration plays a major role in measurement accuracy due to different factors in camera optics such as lens distortions, different camera focal lengths, camera misalignment etc. [21], [22]. Usual checkerboard based camera calibration procedure was carried out to estimate distortion parameters for image rectification [23].

Usual stereo camera calibration is carried out with camera intrinsic and extrinsic parameters [23].Similar to the distortion parameter estimation, a checkerboard pattern is used for stereo camera calibration. Those calibration parameters are later used in the 3D reconstruction process.

2) Stereo image processing: Stereo image processing was used for generating point clouds with true colors mapped from the scanned pipes. The highest intensity points were detected in one image to identify the laser beam points while the other image was searched along the epipolar lines to find the corresponding points. With a circular laser beam, two intersection points were detected along the epipolar lines, which was resolved by carrying out a directional search starting from the center of the image. The image disparity was used for 3D reconstruction [21].

3) RGB mapping: The calculated depth information is used for RGB mapping by stereo calibrating one IR camera with RGB camera and projecting the 3D points on to the color image using Equation (1).

$$\begin{bmatrix} p_x \\ p_y \end{bmatrix} = \begin{bmatrix} s_x & 0 & 0 \\ 0 & 0 & s_z \end{bmatrix} \begin{bmatrix} P_x \\ P_y \\ P_z \end{bmatrix} + \begin{bmatrix} c_x \\ c_z \end{bmatrix} \quad (1)$$

where, (P_x, P_y, P_z) are the 3D real world coordinates, (p_x, p_y) defines the color camera image coordinates, s is an arbitrary scale factor and c is an arbitrary offset.

Once the 3D point is projected on the color image the RGB values of the mapping location are taken and embedded with the generated point cloud. A high-level implementation of the algorithm in pseudo-code is given in Appendix Algorithm 1.

4) Defects detection and mapping: Defects in terms of a color heat-map and ovality are estimated through the detection of the center of the pipe followed by ray casting. Through experimentation, it was discovered that the existing image processing functions available in OpenCV such as Hough Circle detection were too noisy and not accurate enough to detect the center of the pipe on captured laser profile images due to lighting changes with defects and other various surface irregularities. Therefore, the following novel approach was developed and implemented to detect the circle on the image as well as its center.

Firstly, we converted the image into a distance transform map by using the gray-scale values. Then, using matrix operations we approximately identified a circle diameter to generate a dummy circle at the center of the image. Next, we extracted and added the distant transform values along the generated circle circumference. By iteratively changing the position of the circle and its radius, the algorithm searched for the minimum summation of distance transform values along the circle circumference using an optimization algorithm.

Let camera image matrix be $I_{h,w}$ where height is h and width is w. Using Chebyshev distance transform function Dt, the image distance transform matrix $D_{h,w}$ can be defined as:

$$D_{h,w} = Dt(I_{h,w}) \quad (2)$$

For any given two points, the difference of x coordinate is Δx and the difference of y coordinate is Δy, then Chebyshev distance $D_{h,w}$ matrix calculated as;

$$\sum_{i,j} D_{h,w}(x,y) = \sum_{i=1}^{h} \sum_{j=1}^{w} \left[max_{i,j} \left(|\Delta x_i| \ , \ |\Delta y_j| \right) \right] \quad (3)$$

When the circle center denoted by x_c, y_c and radius denoted by r_c. Search initialization values are as in (4, 5, 6).

$$x_c = w/2 \quad (4)$$

$$y_c = h/2 \quad (5)$$

$$r_c = [max(I_w) - min(I_w)]/2 \quad (6)$$

Using Equation (7) the coordinates (P) of the circle circumference are generated where x_i, y_i taken as a single coordinate.

$$(x_i - x_c)^2 + (y_i - y_c)^2 = r_c^2 \quad (7)$$

Now the distance transform values $(V_1, V_2, ..., V_n)$ in the distance transform map D that belongs to the circle circumference coordinates P is used to calculate the total sum T.

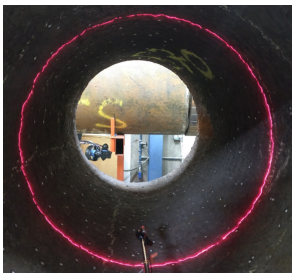

(a) The laser projection view before circle fitting.

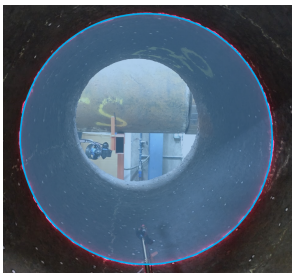

(b) Projection of the optimum circle found by the algorithm.

Fig. 1: Circle fitting.

$$V = D(P) \quad (8)$$

$$T = \sum_{i=1}^{n} (V_i) \quad (9)$$

The best fitting circle $C_{optimum}$ is found by minimizing T.

$$C_{optimum} = \underset{x_c, y_c, r_c}{argmin}(T \mid x_c, y_c, r_c) \quad (10)$$

Fig. 1 shows an example results of the optimal circle detection algorithm. The optimum circle parameters are then used by a custom ray casting algorithm based on a dynamic range parameter to manage computational complexity (Appendix Fig. 2).

Let, x_1, y_1 be the starting point of the scan range (S) and x_2, y_2 be the end point of the scan range. By defining the equation of the line with x, y and changing the angle (θ), rays can be casted around the circle.

$$x_1 = x_c + [(r_c - S/2) \times cos\ \theta] \quad (11)$$

$$y_1 = y_c + [(r_c - S/2) \times sin\ \theta] \quad (12)$$

$$x_2 = x_c + [(r_c + S/2) \times cos\ \theta] \quad (13)$$

$$y_2 = y_c + [(r_c + S/2) \times sin\ \theta] \quad (14)$$

$$x - x_1 = \left[\frac{y_2 - y_1}{x_2 - x_1} \right] (y - y_1) \quad (15)$$

The optimized ray casting algorithm can be used to cast rays around the laser projection to scan and identify the surface anomalies when generating the point cloud. Appendix Fig. 3 shows an example of a ray casting in a zoomed IR image.

Most of the lasers tend to create a thick laser line on the projected surface due to the reflection properties of the surface and defects (Appendix Fig. 3). The extracted distance transform values are fitted with a Gaussian kernel to identify the midpoint of the thick laser line projection as in,

$$G(x) = \sum_{i=1}^{n} \frac{1}{\sigma\sqrt{2\pi}} \times \exp\left[\left(-\frac{1}{2} \left(\frac{(x-\mu)}{\sigma} \right) \right)^2 \right] \quad (16)$$

where, μ is the mean, σ is the standard deviation, x is the intensity variation, and i is the number of terms to be

determined (assumed 4).

The highest intensity point was used to calculate the distance to the center. It was compared with the average radius to identify defects and hence to generate the defects heat-map. A high-level implementation of the algorithm is demonstrated in pseudo-code algorithm as in Appendix Algorithm 3.

5) Orientation detection: We have implemented the iterative closest point (ICP) algorithm [24], [25] to detect the orientation of the robot by comparing the point clouds generated in laser profile scans.

First, we took a base point cloud (P) which was with an estimated orientation by a correctly aligned robot. Then, we took a point cloud (Q) with unknown orientations to find the corresponding pairs of points (p_i, q_j) by searching for the nearest points that aligned between the two point clouds.

$$P = \{p_1 \ldots\ldots\ldots p_n\} \quad ; \quad Q = \{q_1 \ldots\ldots\ldots q_m\} \tag{17}$$

$$(p_i, q_j) = \underset{i,j}{argmin}\left((x_{p_i} - x_{q_i})^2 + (y_{p_i} - y_{q_i})^2 + (z_{p_i} - z_{q_i})^2\right) \tag{18}$$

Then, we minimized the summation of the squared error of rotation (R) and translation (t) of those corresponding points to estimate the transformation parameters.

$$E(R,t) = \sum_{i=1,\ j=1}^{n,m} |p_i \ - Rq_j \ - t|^2 \tag{19}$$

It was further optimized by taking the center of the circle as the center of the mass in the corresponding points of both sets (M_Q, M_P) to generate a new point data set as,

$$M = M_p - M_Q \tag{20}$$

$$p_i^{'} = \{p_i - M\} \tag{21}$$

$$E^{'}(R) = \sum_{i=1,\ j=1}^{n,m} |p_i^{'} \ - Rq_j|^2 \tag{22}$$

$$R_{optimum} = \underset{R}{argmin}(E'|R) \tag{23}$$

A high level implementation of the algorithm is demonstrated in pseudo-code as in Appendix Algorithm 2.

III. Hardware Setup and Software Architecture

The mini-PIRO (mini Pipe Inspection Robot) system was developed under the Sydney Water funded project, "Development of sensor suites and robotic deployment strategies for condition assessment of concrete sewer walls". It has two main parts: a robotic platform and sensor suite. The robotic platform was equipped with basic pipeline inspection functionalities such as tethered remote control, navigation inside pipes with little water puddles, CCTV inspection with a flashlight system. The robot is powered and controlled through a 120m long tether connected to a control station. The sensor suite consists of an IR laser, cameras and an on-board computer (see Fig. 2).

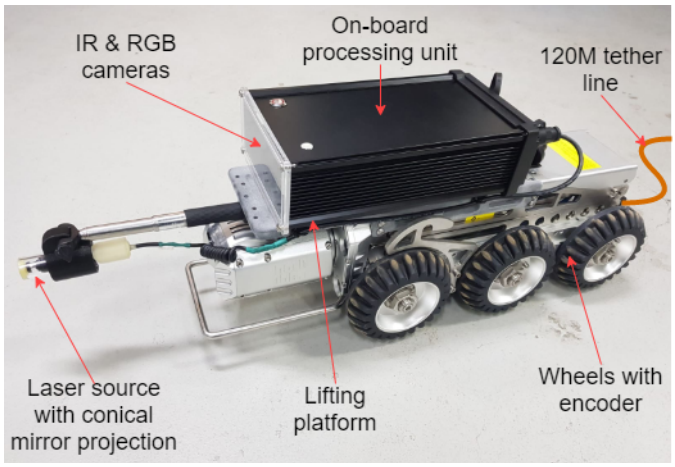

Fig. 2: The mini-PIRO with sensors.

A. Sensor suite

The laser probe was mounted at the front end of the robot using a length adjustable rod. It uses an IR laser (within the wave length of the camera) and a conical mirror to project the circular laser line perpendicular to the pipe wall. An RGB camera with an IR block filter was used so that the laser ring did not appear in the RGB camera. All three cameras were configured to 1280×720 resolution to extract high definition images at a rate of 30 frames per second. The two IR cameras were used to detect the laser ring projection in the captured images and to generate the stereo processed point clouds whereas the RGB camera was used to capture the color information of the associated data points.

As the mini-PIRO is operating in dark underground pipes, the quality of RGB-D mapping is dependent on camera exposure, laser intensity and the robot lighting system which are all remotely adjustable. An encoder with 1000 pulses/revolution was utilized to robot localization. Although, encoders have long term bias with location estimates, in this application, they are reasonable given the water utilities require short map segments. The algorithms were implemented on a high-performance motherboard with an Intel 2.5GHz quad-core processor, 8GB RAM and a 500GB SSD internal storage memory. The system was tested extensively and operates smoothly over a long period of time. The whole unit was secured from possible splashes of water to protect the hardware.

B. Software Architecture

The software architecture (Appendix Fig. 4) was implemented using the Robotic Operating System (ROS) framework based on C++ language and OpenCV libraries for image processing. The computationally heavy functions in the code have been modularized and distributed among ROS nodes to work in parallel as separate threads to improve the real-time performance. The raw image frames taken from the cameras were processed with pre-calibrated camera parameters and algorithms implemented using the OpenCV framework that generates the 2D point cloud of the laser ring that contains the RGB-D vectors. Using the

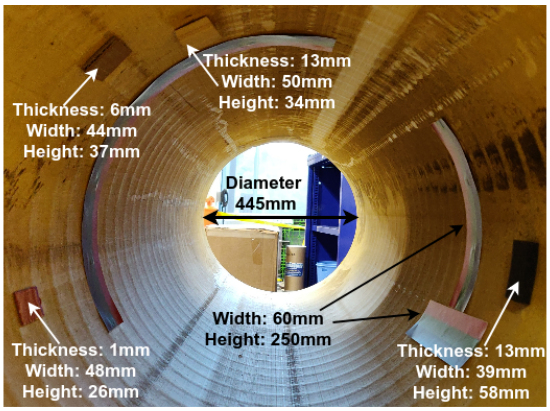

Fig. 3: Storm water pipe with artificial defects with benchmarks is used in the laboratory setup to validate the sensing performance.

odometry, the 2D point clouds generated were iteratively combined to generate the 3D map of the pipe surface. The final results can be visualized in real-time using ROS RVIZ like visualizing tools. The system was automated using Linux automation scripts for a single push button start up.

IV. Experiments & Results

The sensor suites and the algorithms were tested and validated through a set of experiments conducted in different lab setups and in a utility-owned pipe section. The purpose of these experiments were to validate the accuracy of 3D map measurements, RGB depth mapping, defects mapping, orientation detection, real-time performance of laser profiling and evaluating the robustness of the system.

A. Sensor suite validation

To validate the sensors, a storm water pipe was fitted with artificial defects with known dimensions placed around the pipe surface. Figures 3, 4f and 4g show the lab test environment. Artifacts with known dimensions (Fig. 4g) were attached to the internal pipe surface to validate the measurements by comparing it with the ground truth (Fig. 3). Different color stripes (red, green and blue) were placed on the pipe surface as shown in Fig. 3 to validate the color alignment.

The metric scaled point clouds generated from the proposed sensor module are shown in Fig. 4. Fig. 4a shows the RGB depth point cloud generated from the proposed system and Fig. 4b shows the unwrapped version of the point cloud generated using an unroll algorithm. The measurements are validated by comparing the point cloud measurements with the actual measurements taken using tape measure, laser distance measure (DeWalt DW03101-XJ) and vernier caliper. Figure 4d and 4e show some of the measurements taken at different locations.

B. Measurements validation

Table I demonstrates the most significant validations done on the generated point cloud by comparing the point cloud measurements with the known dimensions of the

Location	Physical measurement (mm)	Point cloud measurement (mm)	Error (mm)
Pipe diameter	445	445.36	0.36
Fig. 4d Point 1	13	13.56	0.56
Fig. 4d Point 2	6	6.05	0.05
Fig. 4d Point 3	1	1.68	0.68
Fig. 4d Point 4	14	31.15	17.15
Fig. 4e Point 0-1	500	501.38	1.38
Fig. 4e Point 2-3	250	251.86	1.86
Fig. 4e Point 3-4	60	61.4	1.4
Fig. 4e Point 5-6	250	254.25	4.25
Fig. 4e Point 7-8	60	63.56	3.56
Fig. 4e Point 9-10	60	64.02	4.02
Fig. 4h right defect			
• Height	110	111.31	1.31
• Length	110	109.72	2.78
Fig. 4h left defect			
• Height	110	107.87	2.13
• Length	110	115.16	5.16

TABLE I: Evaluating the measurements of the artificial defects placed on the pipe surface.

defects placed on the pipe. Several points were randomly selected from the region of interest in the generated 3D point clouds using a point cloud analytical tool and the averaged out measurements were compared with the physical measurements. In general, the thickness measurements were accurate to the millimeter level with some exceptions. For example, point 4 in Fig.4d is erroneous, which is due to dark color surface. The dark color surface absorbs most of the projected IR laser light causing poor camera images. Figure 4e and Table I show that points 0 to 4 measurements taken along the circumference of the surface (on the x-axis of the image) are accurate to the millimeter level. However, points 5 to 10 (measurements were taken on the y-axis of the image) have higher errors which are due to the basic odometry received from the lateral movement of the robot. Our future works involves improvements to the robot localization to address these errors. The last 2 rows in the Table I (right defect and left defect locations) show the comparison results taken from the figure 4h point cloud measurements compared with the ground truth that reflects the accuracy of the readings. Fig. 4a show that the colors of the point cloud are well aligned with the locations of the defects and therefore the RGB-depth mapping is accurate to the millimeter level.

Figure 4c shows the severity of the defect in which a color gradient has been applied throughout the point cloud to easily identify defects where yellow end of the spectrum indicates normal and when it goes towards red end of the spectrum the severity of the defect increases. This is the most crucial information for a Sydney Water engineer to identify and repair defects in the scanned pipeline by measuring the defects from the generated point cloud up to millimeter level accuracy. Further information such as wave-like patterns are visible in the representation as seen in Appendix Fig. 5 which were previously discussed in [26].

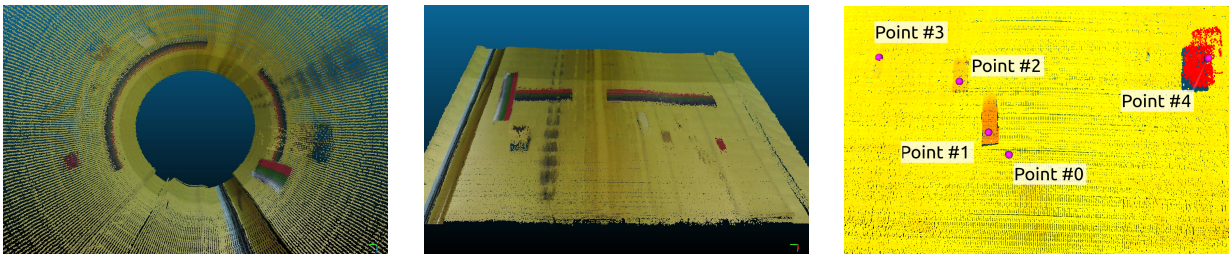

(a) RGB depth point cloud generated from the validation test pipe scan.

(b) The unwrapped RGB depth point cloud generated from the laser profile.

(c) The unwrapped 3D point cloud with the defects heat-map.

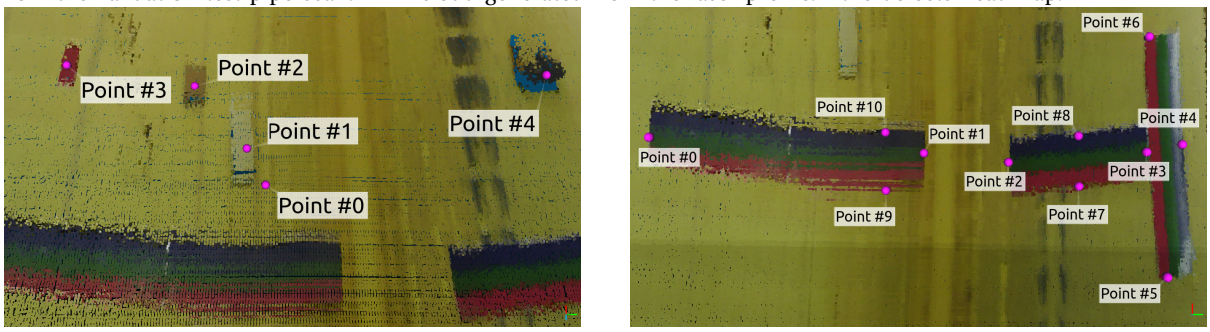

(d) Point cloud defects thickness measurements

(e) Point cloud defects size measurements

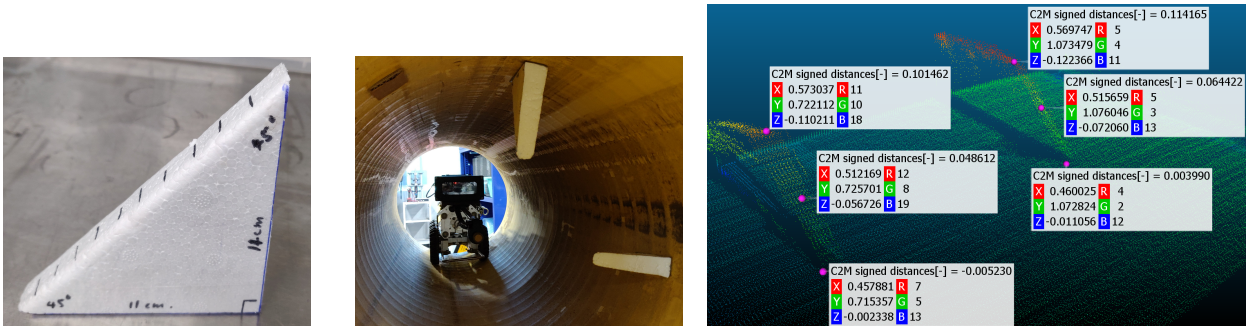

(f) Triangle shaped artificial defect profile made with styrofoam

(g) Lab pipe scan with the styrofoam artificial defects

(h) 3D point cloud measurements of the styrofoam artificial defects

Fig. 4: 3D point cloud measurement accuracy validation.

C. Performance evaluation with existing technologies

Following summarizes our comparative study with existing methods. A corroded metal pipe of diameter 600 mm extracted from the Sydney water network was used to perform these tests (Fig. 5a). We scanned the pipe using a commercially available 3D scanner "Creaform EXAscan SYS-H3D-EXAD" [27] with industry specification of 0.1mm accuracy (Fig. 5b), research work based on existing literature [17]–[19] with 7mm accuracy and our proposed method with 1mm accuracy (Fig. 5c). Figure 5d, 5e shows the comparisons of all three 3D scan models. Fig. 5f shows the heat-map highlighting the defects that overlays on the mesh generated from the proposed system.

D. Orientation validation

Following tests were carried out to validate the algorithms discussed in section II-.5. As shown in Fig. 6 different point clouds have been generated by projecting the laser beam with known angles inside the pipe: first instance - Base scan is taken as the reference, second and third instances - individual rotations of 10 degrees for the Y and Z axes respectively, fourth instance - rotated in both Y and Z axes by 10 degrees each, final instance - rotated along X-axis by 10 degrees.

Physical Orientation (Degrees)	Z Rotation Detection (Degrees)	Y Rotation Detection (Degrees)	X Rotation Detection (Degrees)
Y – 10	-0.0025866	9.851	-0.015133
Z – 10	-9.8511	0.0025376	0.014715
Y & Z – 10	7.0537	7.0008	0.43202
X – 10	-0.000003	-0.000003	0.021256

TABLE II: Evaluating the measurements of the orientation algorithm.

The generated data have been fed into the algorithm and the results have been compared with the known measurements to estimate the accuracy as shown in Table II.

According to the comparisons, individual axis (pitch, yaw) rotations are accurate with just 0.2-degree error. When there's a rotation in both pitch (Y) and yaw (Z) axes at the same time the error goes up to 3 degrees. The rotation in the roll (x) axis is ignored as it cannot be detected accurately because of the symmetrical shape of the circular point cloud.

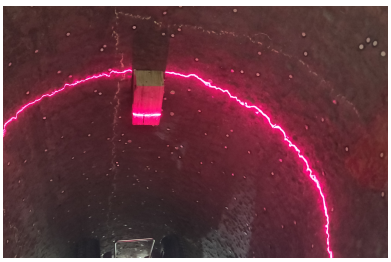

(a) Corroded metal pipe extracted from a Sydney water network. The red laser has been used instead of IR for image demonstration purposes.

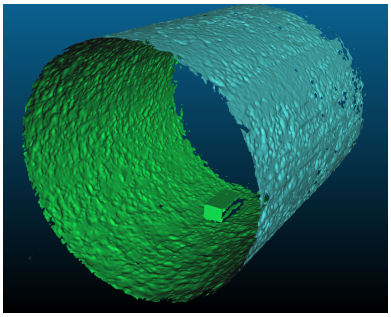

(b) 3D scan generated from the Creaform handheld 3D scanner.

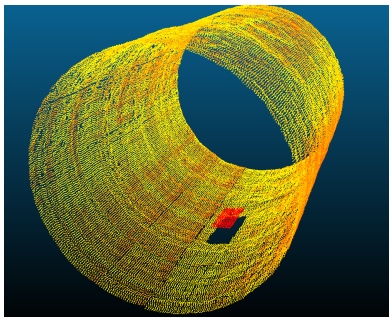

(c) Laser scan generated from the proposed system.

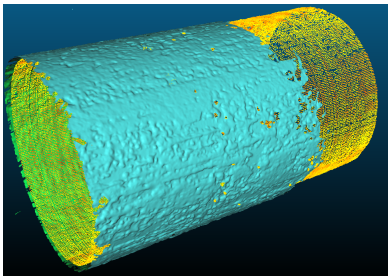

(d) 3D scan and laser scan results comparisons.

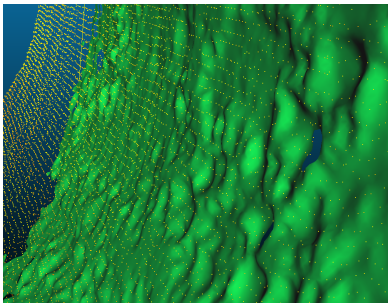

(e) Measurement comparisons.

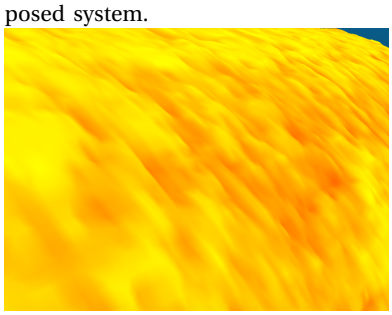

(f) Point cloud to mesh feature validation.

Fig. 5: Ground-truth validation with an industrial 3D laser-scanner.

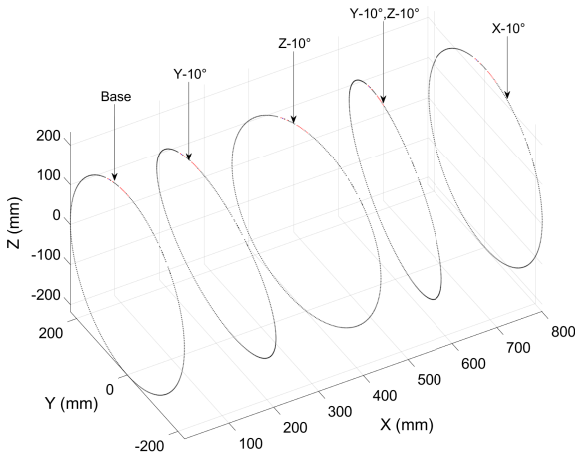

Fig. 6: Test data generated from the laser profile scans with fixed known angles to validate the orientation detection.

E. Field trials and data

The robot was tested in field trials, several Sydney underground water pipe networks to assess its robustness and performance (Fig. 7). The results of the robot is being used to test 60m long spray liner coated pipelines (Fig. 7a, 7b) which had shiny surface and a 60m long CIPP (Cured In Place Pipe) lined pipes (Fig. 7d) with a relatively rough surface are shown in the figures. And the scan results are shown in respective figures (Fig. 7c, 7e, 7f).

F. Real-time performance

The system has been implemented in ROS to capture capture images in 30 fps from all 3 cameras. The robot runs an average speed of 0.2m per second while generating a real-time point cloud. When an in-depth inspection becomes necessary, the robot can run at a slower speed as detailed in [26]. As an example, the areas with apparent corrosion as in figures 7b and 7c may need more attention.

V. Conclusion And Future Work

In this article, we have reported the design and development of a robotic sensing system for RGB-D mapping inside drinking water pipes. We utilized an IR stereo camera vision system and IR laser-pattern projection-based sensing system along with encoders for robot localization. The data gathered are used to build true color 3D maps identifying defects and achieving millimeter level accuracy. The system was first comprehensively tested in laboratory settings followed by field trials in the drinking water pipeline located at Sydney city, Australia. The experimental results indicated that the generated 3D map of the internal pipe surface is with a millimeter level accuracy and can efficiently detect defects and surface corrosion.

The current version of the robotic sensing system was developed for pipes ranging from 400mm to 700mm diameter. In the future, we are planning to miniaturize the system to deploy in pipes with diameters less than 400mm. Further research is planned to solving the measurement inaccuracies relating to dark surfaces by utilizing high intensity lasers. Further work is planned for integrating ultrasound sensing technology for measuring the thickness of water pipe linings.

Acknowledgment

This paper is an outcome from the Smart Linings for Pipes and Infrastructure project funded by the Aus-

(a) Laser profiling in an actual underground water pipeline.

(b) Camera image of the underground water pipeline with spray liner coating.

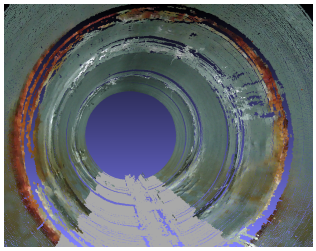

(c) 3D point cloud generated on the underground water pipeline spray liner coating.

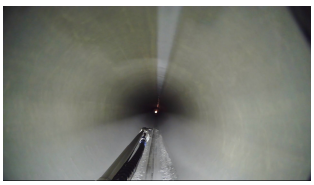

(d) Camera image of an actual underground water pipeline with CIPP liner coating.

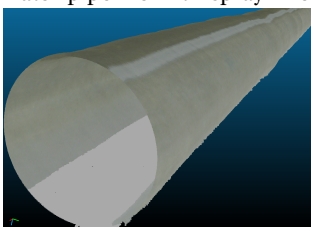

(e) 3D mesh of the CIPP pipe liner coating.

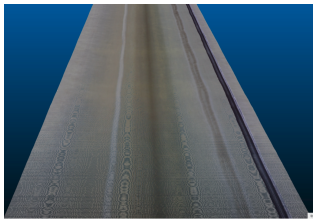

(f) Unwrapped 3D mesh of the underground water pipe sample.

Fig. 7: Field trials with 3D scan results.

tralian Federal Government through the Cooperative Research Centres Projects (CRC-P) grant. The CRC-P Program supports industry-led collaborations between industry, researchers and the community. This CRC-P program is led by the Water Services Association of Australia in collaboration with 34 collaborative partners including researchers, water utilities and industry partners. The reported work is a part of the sub-project 3 on Smart Sensing led by the University of Technology Sydney. The sub-project 3 partners are Abergeldie Watertech Pty Ltd, Bisley & Company Pty Ltd, Calucem, Central SEQ Distributor-Retailer Authority (Urban Utilities), Downer Pty Ltd, Insituform Pacific Pty Ltd, Interflow Pty Ltd, GeoTree Solutions, Parchem Construction Supplies Pty Ltd, Sanexen Environmental Services, South Australian Water Corporation, South East Water Corporation, Sydney Water Corporation, University of Technology Sydney, Ventia Pty Ltd, Water Corporation and Water Services Association of Australia.

Special thanks to Sydney Water funded project, Development of sensor suites and robotic deployment strategies for condition assessment of concrete sewer walls for making the robot and sensors available for this work and Sydney Water for facilitating to carry out field trials.

REFERENCES

[1] J. Valls Miro, N. Ulapane, L. Shi, D. Hunt, and M. Behrens, "Robotic pipeline wall thickness evaluation for dense nondestructive testing inspection," *Journal of Field Robotics*, vol. 35, no. 8, pp. 1293–1310, 2018.

[2] K. Thiyagarajan, S. Kodagoda, R. Ranasinghe, D. Vitanage, and G. Iori, "Robust Sensor Suite Combined with Predictive Analytics Enabled Anomaly Detection Model for Smart Monitoring of Concrete Sewer Pipe Surface Moisture Conditions," *IEEE Sensors Journal*, vol. 20, no. 15, pp. 8232–8243, 2020.

[3] K. Thiyagarajan, S. Kodagoda, R. Ranasinghe, and G. Iori, "Robust sensing suite for measuring temporal dynamics of surface temperature in sewers," *Scientific Reports*, vol. 8, 10 2018.

[4] K. Thiyagarajan, S. Kodagoda, and J. K. Alvarez, "An instrumentation system for smart monitoring of surface temperature," in *2016 14th International Conference on Control, Automation, Robotics and Vision (ICARCV)*, 2016, pp. 1–6.

[5] K. Thiyagarajan, S. Kodagoda, L. V. Nguyen, and R. Ranasinghe, "Sensor Failure Detection and Faulty Data Accommodation Approach for Instrumented Wastewater Infrastructures," *IEEE Access*, vol. 6, pp. 56 562–56 574, 2018.

[6] L. Chun-Lei, S. Hao, L. Chun-Lai, and L. Jin-Yang, "Intelligent detection for tunnel shotcrete spray using deep learning and lidar," *IEEE Access*, vol. 8, pp. 1755–1766, 2020.

[7] Z. Li, P. C. Gogia, and M. Kaess, "Dense surface reconstruction from monocular vision and lidar," in *2019 International Conference on Robotics and Automation (ICRA)*, 2019, pp. 6905–6911.

[8] J. Zhang, Z. Lu, W. Li, and Q. Liao, "A robust and fast 3d face reconstruction method using realsense camera," in *2017 International Conference on Wireless Communications, Signal Processing and Networking (WiSPNET)*, 2017, pp. 2691–2695.

[9] J. Feulner, J. Penne, E. Kollorz, and J. Hornegger, "Robust real-time 3d modeling of static scenes using solely a time-of-flight sensor," in *2009 IEEE Computer Society Conference on Computer Vision and Pattern Recognition Workshops*, 2009, pp. 74–81.

[10] S. M. Ayaz, D. Khan, and M. Y. Kim, "3d handheld scanning based on multiview 3d registration using kinect sensing device," in *2017 IEEE International Conference on Multisensor Fusion and Integration for Intelligent Systems (MFI)*, 2017, pp. 330–335.

[11] M. Nasrollahi, N. Bolourian, Z. Zhu, and A. Hammad, "Designing LiDAR-equipped UAV platform for structural inspection," in *35th International Symposium on Automation and Robotics in Construction and International AEC/FM Hackathon: The Future of Building Things, ISARC 2018*. Department of Building, Civil and Environmental Engineer, Concordia University, Canada: International Association for Automation and Robotics in Construction I.A.A.R.C), 2018.

[12] Z. Liu and D. Krys, "The use of laser range finder on a robotic platform for pipe inspection," *Mechanical Systems and Signal Processing*, vol. 31, pp. 246–257, 2012.

[13] J. Saenz, N. Elkmann, T. Stuerze, S. Kutzner, and H. Althoff, "Robotic systems for cleaning and inspection of large concrete pipes," in *2010 1st International Conference on Applied Robotics for the Power Industry, CARPI 2010*, Fraunhofer IFF, 39106 Magdeburg, Germany, 2010.

[14] O. Duran, K. Althoefer, and L. D. Seneviratne, "Automated pipe defect detection and categorization using caniera/laser-based profiler and artificial neural network," *IEEE Transactions on Automation Science and Engineering*, vol. 4, no. 1, pp. 118–126, 2007.

[15] J.-S. Yoon, M. Sagong, J. S. Lee, and K.-s. Lee, "Feature extraction of

a concrete tunnel liner from 3D laser scanning data," *NDT and E International*, vol. 42, no. 2, pp. 97–105, 2009.

[16] R. Rantoson, C. Stolz, D. Fofi, and F. Mériaudeau, "Non contact 3D measurement scheme for transparent objects using UV structured light," in *2010 20th International Conference on Pattern Recognition, ICPR 2010*, Laboratoire Le2i-CNRS UMR 5158, Université de Bourgogne, 12, Rue de la Fonderie, 71 200 Le Creusot, France, 2010, pp. 1646–1649.

[17] J. Kofman, J. T. Wu, and K. Borribanbunpotkat, "Multiple-line full-field laser-camera range sensor," in *Optomechatronic Computer-Vision Systems II*, vol. 6718, Dept. Systems Design Engineering, University of Waterloo, Waterloo, ON N2L 3G1, Canada, 2007.

[18] N. Stanić, M. Lepot, M. Catieau, J. Langeveld, and F. Clemens, "A technology for sewer pipe inspection (part 1): Design, calibration, corrections and potential application of a laser profiler," *Automation in Construction*, vol. 75, pp. 91–107, 2017.

[19] M. Lepot, N. Stanić, and F. H. L. R. Clemens, "A technology for sewer pipe inspection (Part 2): Experimental assessment of a new laser profiler for sewer defect detection and quantification," *Automation in Construction*, vol. 73, pp. 1–11, 2017.

[20] E. Ujkani, J. Dybedal, A. Aalerud, K. B. Kaldestad, and G. Hovland, "Visual Marker Guided Point Cloud Registration in a Large Multi-Sensor Industrial Robot Cell," in *14th IEEE/ASME International Conference on Mechatronic and Embedded Systems and Applications, MESA 2018*. Department of Engineering Sciences, Mechatronics Group, University of Agder, Norway: Institute of Electrical and Electronics Engineers Inc., 2018.

[21] L. R. Ramírez-Hernández, J. C. Rodríguez-Quiñonez, M. J. Castro-Toscano, D. Hernández-Balbuena, W. Flores-Fuentes, R. Rascón-Carmona, L. Lindner, and O. Sergiyenko, "Improve three-dimensional point localization accuracy in stereo vision systems using a novel camera calibration method," *International Journal of Advanced Robotic Systems*, vol. 17, no. 1, p. 1729881419896717, 2020. [Online]. Available: https://doi.org/10.1177/1729881419896717

[22] G. Ning, L. Lei, Y. Feng, and L. Tongtong, "Binocular stereo vision calibration based on constrained sparse beam adjustment algorithm," *Optik*, vol. 208, p. 163917, 2020. [Online]. Available: http://www.sciencedirect.com/science/article/pii/S0030402619318157

[23] S. Yang, Y. Gao, Z. Liu, and G. Zhang, "A calibration method for binocular stereo vision sensor with short-baseline based on 3d flexible control field," *Optics and Lasers in Engineering*, vol. 124, p. 105817, 2020. [Online]. Available: http://www.sciencedirect.com/science/article/pii/S0143816619301691

[24] P. Li, R. Wang, Y. Wang, and W. Tao, "Evaluation of the icp algorithm in 3d point cloud registration," *IEEE Access*, vol. 8, pp. 68 030–68 048, 2020.

[25] B. Bellekens, V. Spruyt, R. Berkvens, R. Penne, and M. Weyn, "A benchmark survey of rigid 3d point cloud registration algorithms," *International Journal On Advances in Intelligent Systems*, vol. 1, 06 2015.

[26] A. Gunatilake, L. Piyathilaka, S. Kodagoda, S. Barclay, and D. Vitanage, "Real-Time 3D Profiling with RGB-D Mapping in Pipelines Using Stereo Camera Vision and Structured IR Laser Ring," in *2019 14th IEEE Conference on Industrial Electronics and Applications (ICIEA)*, 2019, pp. 916–921.

[27] Creaform, "Exascan 3d scanner," www.creaform3d.com, 2015, https://www.creaform3d.com/en/customer-support/legacy-products/exascan-scanner#gref [Accessed 26 Oct. 2020].

Amal Gunatilake (Student Member, IEEE) received the B.Eng. (Hons.) degree in software engineering from the University of Westminster, UK, in 2013, and the diploma in electrical and electronic engineering from the Arthur C. Clark Institute for Modern Technologies, Sri Lanka, in 2007.

He has worked over 5 years in the open-source software engineering industry as a Senior Software Engineer to research and develop IoT software products. He is currently pursuing his Ph.D. degree in robotics from the University of Technology Sydney, Australia. His current research interests include perception, SLAM using unconventional sensors, and infrastructure robotics. He is in the Executive Committee of the IEEE Sensor Council New South Wales chapter, Australia in 2020.

Lasitha Piyathilaka (Member, IEEE) received B.Sc.Eng (Hons.) degree in 2004 (Electrical engineering), M.Phil. in 2011 from University of Moratuwa, Sri Lanka and Ph.D. in 2016 (robotics) from University of Technology Sydney. He has years of industry experience and has worked in several university-industry collaboration projects.

Currently, he is a lecturer at Central Queensland University (CQU) and previously worked as a Research Fellow at University of Technology Sydney (UTS) where he led an engineering team to develop sensing and robotic systems to inspect underground infrastructure.

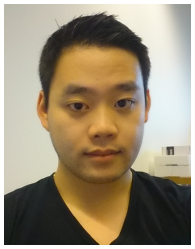

Antony Tran received the B.E degree in mechanical and mechatronic engineering in 2014, and Ph.D. in 2019 from the University of Technology Sydney, Sydney, Australia.

He is currently working in the iPipes Lab, UTS Robotics Institute at the University of Technology Sydney. His research interests include intuitive interfaces, collaborative human robot interaction and safety in human-robot collaboration.

Vinoth Kumar Viswanathan received the B.E. degree in electronics and communications engineering from the Anna University, India in 2008 and MSc. degree specializing in automation and control from National University of Singapore in 2012.

He has worked as a Research Engineer and Mechatronics Engineer on various industry funded projects at National University of Singapore, Singapore University of Technology and Design and University of Technology Sydney (UTS). Currently, he is a Mechatronics Engineering Lead at the iPipes Lab, UTS Robotics Institute, UTS, Australia.

His research interests include mechatronics systems design, pipeline inspection robotics, underwater systems, soft robots and aerial vehicles. He works at the interface of mechanical systems and sensing tools for practical applications.

Karthick Thiyagarajan (Member, IEEE) received the B.E. degree in electronics and instrumentation engineering from the Anna University, Chennai, India, in 2011, the M.Sc. degree in mechatronics from the University of Newcastle Upon Tyne, Newcastle Upon Tyne, U.K., in 2013, and the Ph.D. degree specializing in smart sensor technologies from the University of Technology Sydney, Sydney, Australia, in 2018.

He is currently a Research Fellow and Smart Sensing Technologies Research Lead with the iPipes Lab, UTS Robotics Institute, University of Technology Sydney, Australia. His current research interests include smart sensing technologies, infrastructure robotics, and sensor analytics.

Dr. Thiyagarajan is also serving as a Treasurer for the IEEE Sensors Council New South Wales Chapter, Australia, in 2020, an Executive Committee Member of the IEEE Instrumentation and Measurement Society New South Wales Chapter, Australia, in 2020.

Sarath Kodagoda (Member, IEEE) received the B.Sc. Eng. (Hons.) degree in electrical engineering from the University of Moratuwa, Sri Lanka, in 1995, and the M.Eng. and Ph.D. degrees in robotics from Nanyang Technological University, Singapore, in 2000 and 2004, respectively.

He is currently a Professor, an Acting Director of the UTS Robotics Institute, the Founder of the iPipes Lab, and a Program Coordinator of the Mechanical and Mechatronics degree at the University of Technology Sydney, Australia. His current research interests include infrastructure robotics, sensors and perception, machine learning and human-robot interaction.